PNAS RESEARCH ARTICLE | NEUROSCIENCE

Green fluorescent cAMP indicator of high speed and specificity suitable for neuronal live-cell imaging

Seiko Kawata[a], Yuki Mukai[a], Yumi Nishimura[a], Tomoyuki Takahashi[b], and Naoto Saitoh[a,1]

Edited by Joseph Beavo, University of Washington School of Medicine, Seattle, WA; received December 15, 2021; accepted April 29, 2022

Cyclic adenosine monophosphate (cAMP) is a canonical intracellular messenger playing diverse roles in cell functions. In neurons, cAMP promotes axonal growth during early development, and mediates sensory transduction and synaptic plasticity after maturation. The molecular cascades of cAMP are well documented, but its spatiotemporal profiles associated with neuronal functions remain hidden. Hence, we developed a genetically encoded cAMP indicator based on a bacterial cAMP-binding protein. This indicator "gCarvi" monitors $[cAMP]_i$ at 0.2 to 20 μM with a subsecond time resolution and a high specificity over cyclic guanosine monophosphate (cGMP). gCarvi can be converted to a ratiometric probe for $[cAMP]_i$ quantification and its expression can be specifically targeted to various subcellular compartments. Monomeric gCarvi also enables simultaneous multisignal monitoring in combination with other indicators. As a proof of concept, simultaneous cAMP/Ca^{2+} imaging in hippocampal neurons revealed a tight linkage of cAMP to Ca^{2+} signals. In cerebellar presynaptic boutons, forskolin induced nonuniform cAMP elevations among boutons, which positively correlated with subsequent increases in the size of the recycling pool of synaptic vesicles assayed using FM dye. Thus, the cAMP domain in presynaptic boutons is an important determinant of the synaptic strength.

cAMP | neuron | live cell imaging | indicator

Significance

We have developed a cyclic adenosine monophosphate (cAMP)-specific indicator, gCarvi, having an optimal coverage of neuronal cAMP concentrations. This indicator has a subsecond time resolution and highest cAMP/cGMP specificity. In combination with other signal reporters, gCarvi can reveal dynamic linkages of cAMP with other signal cascades. Ratiometric gCarvi can determine the basal $[cAMP]_i$ in neurons. Hence, gCarvi is a powerful tool for clarifying cAMP dynamics underlying multiple neuronal functions.

Cyclic adenosine monophosphate (cAMP) is a widely conserved second messenger in prokaryotic and eukaryotic cells. In mammalian cells, global and local cAMP concentrations are controlled by the balance of adenylyl cyclases (ACs) (1, 2) and phosphodiesterase (PDE) (3) activities. Cyclic AMP activates effector proteins, including protein kinase A (PKA), exchange protein directly activated by cAMP (Epac), cyclic nucleotide-gated (CNG) channels, or Popeye domain containing proteins (4). Another cyclic nucleotide messenger cyclic guanosine monophosphate (cGMP) activates protein kinase G (PKG) or CNG channels for a variety of cell functions (5). Both cAMP and cGMP are involved in various synaptic modulations (6).

Quantitative live imaging tools were initially developed for Ca^{2+} (7) and subsequently for cAMP by utilizing Förster resonance energy transfer (FRET) (8). Since then, a large number of Ca^{2+} indicators have been developed, which have been used to clarify spatiotemporal Ca^{2+} dynamics (9, 10). Likewise, cAMP indicators (11, 12) have revealed uneven distribution of intracellular cAMP such as nanodomain (13, 14), axonal (15), or dendritic (16, 17) concentration gradients. Cyclic AMP is thought to play essential roles in central synaptic functions (18). However, cAMP probes are still under development for clear-cut imaging of intracellular cAMP dynamics. From a user's perspective, the following properties are desirable for a cAMP indicator: 1) easy expression and detection; 2) wide dynamic range (D.R.) spanning the intracellular cAMP concentration range; 3) high specificity for cAMP over the other nucleotides, particularly cGMP; 4) stable intracellular imaging performance; and 5) no interference with endogenous cAMP pathways.

Hence, we developed a cAMP indicator which can be easily expressed with an adeno-associated virus (AAV) vector and allows imaging in a simple optical system. Most available cAMP indicators are composed of regulatory subunits of the cAMP-binding domain (CBD) of PKA or Epac. Since PKA and Epac are endogenous molecules operating downstream of cAMP, these indicators can potentially interfere with physiological functions of cAMP pathways such as long-term plasticity. Another caveat in cAMP imaging is cross-detection of cGMP. Even with a high cAMP/cGMP selectivity, if a cAMP indicator detects cGMP in the operational range of 0.1 to 3 μM (19–21), it can be a serious problem. Our cAMP indicator is based on the CBD of a bacterial cAMP receptor protein (CRP) (also known as catabolite activator protein [CAP]) (22), which has <30% amino acid homology to mammalian CBDs (23). We fused the CBD to a popular spectrum circular permutated GFP (cpGFP). For an optimal cAMP indicator screening, we

Author affiliations: [a]Department of Neurophysiology, Graduate School of Life and Medical Sciences, Doshisha University, Kyoto, 610-0394, Japan; and [b]Cellular and Molecular Synaptic Function Unit, Okinawa Institute of Science and Technology Graduate University, Okinawa, 904-0495, Japan

Author contributions: N.S. designed research; S.K., Y.M., and Y.N. performed research; and S.K., T.T., and N.S. wrote the paper.

The authors declare no competing interest.

This article is a PNAS Direct Submission.

[1]To whom correspondence may be addressed. Email: nasaito@mail.doshisha.ac.jp.

This article contains supporting information online at http://www.pnas.org/lookup/suppl/doi:10.1073/pnas.2122618119/-/DCSupplemental.

Published July 6, 2022.

considered: 1) the C-helix linker length, 2) cpGFP variants, and 3) linker site substitution in comparison with cAMP and cGMP responses. Our cAMP indicator has a high cAMP/cGMP specificity (D.R. ratio × K_d ratio) of >100 and low affinity to cGMP (K_d = 27 μM). This probe has a subsecond on-rate for cAMP detection, allowing live imaging of intracellular cAMP dynamics with sufficient temporal resolution.

Results

Development of a Green Fluorescent Probe for cAMP. The *Escherichia coli* CRP is a transcriptional activator that regulates many transcription units in response to intracellular cAMP elevation (22). CRP is organized in two distinct domains: 1) an N-terminal CBD (residues 1 to 136), which contains a cyclic nucleotide-binding module and a long α-helix (called C-helix); and 2) a C-terminal DNA-binding domain (DBD; residues 139 to 209), which contains a helix-turn-helix motif for binding to DNA (Fig. 1*A*). The binding of cAMP to the CBD induces a conformational change of the C-helix, thereby enabling the DBD to bind to specific DNA sequences (24, 25). We utilized this molecule as the basis for a cAMP probe, in which the CBD of CRP is fused to cpGFP derived from GCaMP3 (Fig. 1*A*). First, we explored the optimal linker length from the C-helix to the adjacent D-helix (129 to 156 amino acids [aa]) to fuse the cpGFP (*SI Appendix*, Table S1), because Thr-127 and Ser-128 in CRP are required for the cAMP-CBD binding. The CBD-cpGFPs successfully converted the conformational change induced by cAMP binding into the changes in their fluorescence intensity (ΔF). Since an increase in fluorescence with cAMP elevation is preferable for detection, we adopted CBD135-cpGFP (ΔF = +45%) as the lead construct of the cAMP probe. As a next step, we screened cpGFP variants from the recent versions of GCaMPs and G-GECOs (*SI Appendix*, Table S2). Of these candidates with low sensitivity to cGMP, we adopted the G-GECO1 construct having the highest sensitivity (ΔF = +74%) to cAMP.

Since amino acid species in the linker sequence between the ligand-binding domain and fluorescent reporter protein determines the D.R. of ligand detection (26), we mutated the CBD at residue 135 (*SI Appendix*, Table S3). Although substitution to aromatic amino acids provided wide D.R., considering the balance with the sensitivity to cGMP, we selected the A135Y mutant (ΔF = +144%) as an optimal cAMP indicator. We named this cAMP indicator green fluorescent cAMP receptor protein-utilizing validated indicator (gCarvi) (*SI Appendix*, Fig. S1). gCarvi showed no detectable response to nucleotides other than cAMP and cGMP at concentrations up to 1 mM (*SI Appendix*, Fig. S2).

Characteristics of gCarvi. The fluorescence excitation/emission spectra of purified gCarvi protein showed an excitation peak at 504 nm and an emission peak at 523 nm, regardless of the presence or absence of cAMP (Fig. 1*B*; corresponding absorption spectra are shown in *SI Appendix*, Fig. S3*A*). Comparing gCarvi's spectra with those of a fluorescein reference standard, we estimated the molar extinction coefficient (ε) and quantum yield (QY) of gCarvi (*SI Appendix*, Fig. S3*B*). The ε-value of gCarvi in 10 μM cAMP (20,600 M^{-1} cm^{-1}) was half that of Ca^{2+}-bound G-GECO1 (41,000 M^{-1} cm^{-1}), whereas the QY value of gCarvi in 10 μM cAMP (0.79) was twice that of Ca^{2+}-bound G-GECO1 (0.42) (27). Thus, in terms of brightness (εQY), cAMP-bound gCarvi is comparable to Ca^{2+}-bound G-GECO1. The dose–response curve of gCarvi had a maximal cAMP response (F_{max}) of 2.46 ± 0.05 (D.R. = 1.46), and a dissociation

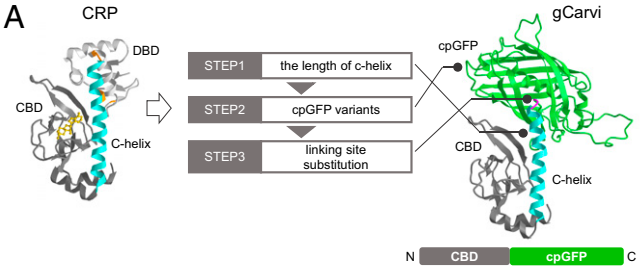

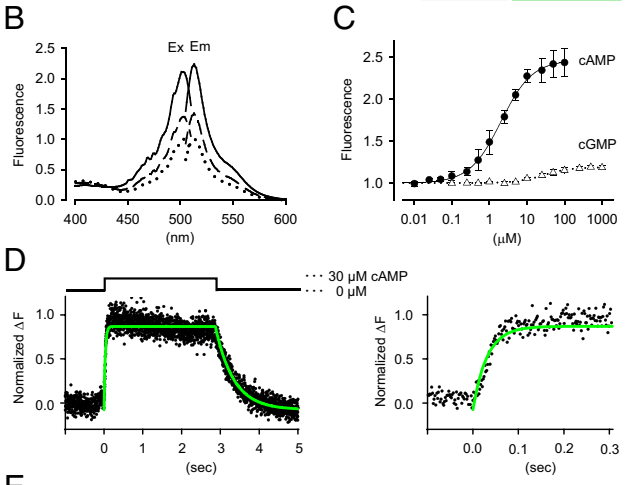

E

	cAMP					cGMP		
	K_d (μM)	*n*	D.R.	k_{on} ($M^{-1}s^{-1}$)	k_{off} (s^{-1})	K_d (μM)	*n*	D.R.
gCarvi	2.03	1.05	1.46	1.38 × 10^6	3.31	27.4	1.22	0.19

Fig. 1. Properties of the green fluorescent cAMP indicator "gCarvi." (*A*) Cyclic AMP indicator, gCarvi, was developed through a three-step screening process. Structure of *E. coli* cAMP receptor protein (CRP, PDB_1G6N), composed of the CBD (gray) and a DBD (light gray) (*Left*). cAMP and C-helix are shown in yellow and light blue, respectively. The positions of 129 aa, 138 aa, and 156 aa in CRP are highlighted in orange. Schematic structure of gCarvi and the predicted three-dimensional (3D) structure using the Phyre2 website (*Right*). CRP 135 aa position (linking site) is highlighted in red. (*B*) Excitation (Ex, *Left*) and emission (Em, *Right*) spectra of purified gCarvi protein in the absence (dotted line) or presence of 3 μM (dashed line) or 10 μM (solid line) cAMP. Each fluorescence spectrum was normalized to the peak fluorescence in the absence of cAMP. (*C*) Dose–response curves of gCarvi protein for cAMP (closed circle) and cGMP (open triangle). Fitting curves for cAMP (solid line) and cGMP (dashed line) were calculated using the Hill equation. Each fluorescence intensity was normalized to the F_{min}. The data represent the means ± SD (*n* = 3 independent experiments). (*D*) Typical time profile of gCarvi kinetics under confocal line scan with microperfusion of 0 or 30 μM cAMP in PBS. gCarvi protein was conjugated to a coverslip via its His-tag. Fitting curves for cAMP binding and unbinding (in green) were calculated with a one-site binding model. Fluorescence was normalized to the F_{min}–F_{max}. On-rate time window is shown on the *Right*. (*E*) Dissociation constant (K_d), Hill constant (*n*), dynamic range (D.R.), and binding constant (k_{on}, k_{off}) of gCarvi are summarized. The dissociation constants for cAMP and cGMP were 2.03 ± 0.22 μM and 27.4 ± 4.4 μM, respectively. The Hill constants for cAMP and cGMP were 1.05 ± 0.11 and 1.22 ± 0.21, respectively. The dynamic ranges for cAMP and cGMP were 1.46 ± 0.05 and 0.19 ± 0.01, respectively. The binding rate and unbinding rate constants for cAMP were 1.38 ± 0.25 × 10^6 M^{-1} s^{-1} and 3.31 ± 0.77 s^{-1} (*n* = 8 independent experiments). All data represent the means ± SD.

constant (K_d) and Hill coefficient (*n*) of 2.03 ± 0.22 μM and 1.05 ± 0.11, respectively, the latter indicating one-to-one binding without allosteric effect. In contrast to cAMP, the responses of gCarvi to cGMP were much weaker, with a F_{max} of 1.19 ± 0.01 (D.R. = 0.19), and a K_d of 27.4 ± 4.4 μM (*n* = 1.22 ± 0.21) (Fig. 1 *C* and *E*). Hence, the cAMP specificity of gCarvi relative to cGMP can be calculated as 106 [(1.46/0.19) × (27.4/2.03)], indicating the highest specificity among cAMP probes reported so far (*SI Appendix*, Table S4). Importantly, the cAMP concentration range detected by this probe (0.2 to 20 μM, Fig. 1*C*) well covers the basal and elevated cAMP concentrations reported in

mammalian neurons (17, 28, 29). Like previously developed cpFP-based probes (26), this cAMP probe is sensitive to pH (*SI Appendix*, Fig. S4*A*); even so, its D.R. was steady at pH 6 to 8 (*SI Appendix*, Fig. S4*B*).

Activation of Ca^{2+}-dependent AC1 in striatal spiny projection neurons can elevate intracellular cAMP within a few seconds (30). The cAMP elevation is also transient because of degradation by PDEs and diffusion out of the cAMP domain formed by localized ACs (30, 31). Little attention has so far been paid to the detection kinetics for cAMP indicators (*SI Appendix*, Table S4), except for the cyclic nucleotide-binding domain of the MloK1 channel (mlCNBD)-FRET probe reported to have fast k_{on} and k_{off} values. However, the K_d value of mlCNBD-FRET calculated from the k_{off}/k_{on} deviates by a factor of >7 from that determined from a dose–response relationship (32). We made kinetics measurements for gCarvi using a microperfusion system combined with line-scan analysis under confocal microscopy (Fig. 1*D*). The apparent kinetic parameters of gCarvi were $k_{on} = 1.38 \pm 0.25 \times 10^6\ M^{-1}\ s^{-1}$ and $k_{off} = 3.31 \pm 0.77\ s^{-1}$, corresponding to a binding time constant of 0.07 s for 10 μM cAMP and unbinding time constant of 0.30 s. The K_d value calculated from the ratio ($k_{off}/k_{on} = 2.49$ μM) nearly coincided with that estimated from the dose–response relationship (2.03 μM, Fig. 1*E*). Thus, this cAMP indicator can reliably monitor cAMP transients at a subsecond resolution. Indeed, in comparison to cADDis, gCarvi indicated faster rise time of cAMP elevation stimulated by a β-adrenergic receptor agonist in COS-7 cells (*SI Appendix*, Fig. S5).

Extension of gCarvi to a Ratiometric cAMP Indicator. Ratiometric imaging uses the ratio between fluorescence intensities of an indicator at two wavelengths in order to cancel out some unwanted variations caused by uneven probe distribution and optical conditions. For quantitative measurements of $[cAMP]_i$, we developed a ratiometric probe from gCarvi. We compared photo-stable red fluorescent proteins, TagRFP and mCherry, by fusing each of them to the gCarvi N terminus and found that fusion of mCherry provided wider D.R. than TagRFP (*SI Appendix*, Table S5). Therefore, we adopted mCherry-CBD A135Y-cpGFP(G-GECO1) as a ratiometric gCarvi (Fig. 2 *A* and *B*). The mCherry-fused ratiometric probe well preserved the cAMP specificity, the wide D.R., the single molecule binding stoichiometry and the binding kinetics of monomeric gCarvi (Fig. 2*C*). This probe was expressed throughout hippocampal neurons using the recombinant AAV-SynTetOff vector (33) (Fig. 2*D*), and was successfully used to monitor $[cAMP]_i$ increase induced by adrenergic receptor activation (*SI Appendix*, Fig. S6*A*) or $[cAMP]_i$ decrease induced by soluble AC inhibition (*SI Appendix*, Fig. S6*B*). Ratiometric gCarvi could be more specifically expressed in targeted subcellular compartments, such as cell nuclei, cell membranes, or axon terminals (*SI Appendix*, Fig. S7). The nuclear and presynaptic targeting constructs had the same D.R. as the nontargeting construct in COS-7 cells, whereas the membrane targeting construct showed 30% smaller D.R. in HEK293T cells (*SI Appendix*, Fig. S8*A*). The presynaptic targeting construct showed cAMP increase at hippocampal presynaptic boutons stimulated by a transmembrane AC (tmAC) activator with a PDE inhibitor (*SI Appendix*, Fig. S8*B*).

Using the nontargeting ratiometric probe, we measured basal $[cAMP]_i$ in cultured hippocampal neurons. Since uneven photobleaching of the two colors in ratiometric gCarvi would directly affect the ratio analysis, we carried out experiments under minimal photobleaching conditions. After permeabilizing neurons with escin (30 μM), neurons were exposed to a range of cAMP concentrations of 1 to 100 μM (Fig. 2*E*). The ratiometric signal fit curve indicated $K_d = 3.20 \pm 0.38$ μM ($n = 1.41 \pm 0.13$) (Fig. 2*F*), comparable to that of the purified ratiometric gCarvi (Fig. 2*C*). The basal $[cAMP]_i$ estimated from this curve fit was 1.38 ± 0.59 μM. This concentration is similar to those reported in mammalian cells (34, 35) and close to the K_d of the ratiometric gCarvi for cAMP binding, allowing quantitative imaging of neuronal $[cAMP]_i$.

Simultaneous cAMP and Ca^{2+} Imaging in Hippocampal Neurons. Cross-regulation of cAMP and Ca^{2+} is involved in various neuronal functions (36). For simultaneous monitoring of both messengers, gCarvi was coexpressed with a red fluorescent Ca^{2+} indicator, jRCaMP1b (37), in cultured hippocampal neurons (Fig. 3*A*). Bath application of a tmAC activator forskolin (FSK, 10 μM) with a PDE inhibitor isobutyl methyl xanthine (IBMX, 100 μM) increased somatic cAMP, which reached a maximal level within ∼3 min (Fig. 3*B*), whereas mCherry-cpGFP without CBD showed no such response (*SI Appendix*, Fig. S9). After washing out FSK/IBMX, the cAMP level returned to the baseline within ∼5 min (Fig. 3*B*). Of 57 neurons tested, 25 showed an increase in spontaneous spikes and basal level of somatic Ca^{2+} during cAMP elevation (Fig. 3 *C*, *D*, *G*, and *H*), and 17 neurons showed only a concomitant tonic increase in Ca^{2+} with cAMP (Fig. 3 *E*, *G*, and *H*). The remaining 15 neurons showed relatively small increases in cAMP in response to FSK/IBMX and no clear change in the level of Ca^{2+} (Fig. 3 *F*, *H*, and *I*). These results suggest that elevation of intracellular cAMP above a certain level can induce tonic Ca^{2+} elevation and then additive Ca^{2+} spikes in hippocampal neurons. Then, might Ca^{2+} elevation induce cAMP elevation? Direct electrical stimulations (5 to 20 Hz, 1-s train) caused frequency-dependent Ca^{2+} rises without detectable increase in cAMP (*SI Appendix*, Fig. S10). Thus, the coupling seems unidirectional only from cAMP to Ca^{2+} in the present experimental condition.

Cyclic AMP Imaging Combined with Synaptic Vesicle Imaging in Presynaptic Terminals. Since cAMP can be involved in presynaptic plasticity at cerebellar granule cell (GC)–Purkinje cell (PC) synapses (38–40), we examined whether presynaptic cAMP elevation might affect synaptic vesicle (SV) recycling in cerebellar granule cell axon terminals in culture, using gCarvi in combination with FM 4-64 SV imaging. Using a human synapsin promoter in rAAV, we expressed gCarvi in cerebellar granule cells (Fig. 4*A*). To avoid the adenosine receptor-inhibiting side effect of IBMX, we used ibudilast as a PDE inhibitor. Bath application of 10 μM FSK with 50 μM ibudilast caused a fast increase of the gCarvi fluorescence in boutons within 1 min (Fig. 4*B*), indicating the boutons have a high tmAC activity–volume ratio. The gCarvi fluorescence at 5 min after bath application ($F_{5\ min}/F_0 = 1.66 \pm 0.25$, Fig. 4*B*) was similar to that in hippocampal soma ($F_{5\ min}/F_0 = 1.77 \pm 0.38$, Fig. 3*B*). After washout of the drugs, cAMP level returned to the baseline in ∼5 min (Fig. 4*C*) similar to hippocampal neurons (Fig. 3*B*). Thus, the magnitude of FSK-induced cAMP concentration changes is comparable to that in hippocampal soma.

To assay SV recycling, we loaded granule cell axon terminals with FM 4-64 (5 μM) in high KCl (72 mM) solution. We then induced cAMP elevations by bath application of FSK/ibudilast. The magnitude of cAMP signal elevations varied among individual boutons (Fig. 4*D* and *SI Appendix*, Fig. S11). Thirty

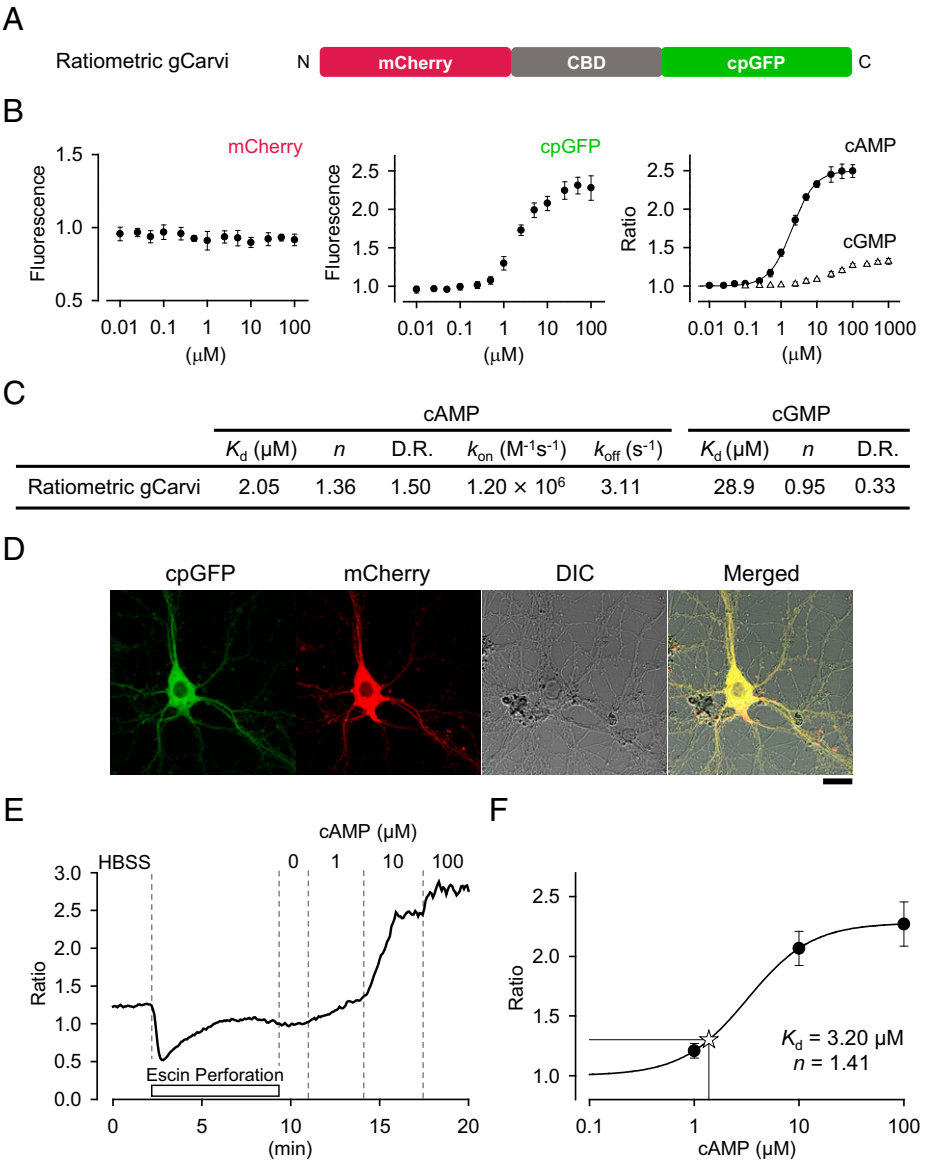

Fig. 2. Ratiometric gCarvi is suitable for quantitative imaging of neuronal cAMP. (*A*) Schematic structure of mCherry fused gCarvi (ratiometric gCarvi) for quantitative measurements of $[cAMP]_i$. (*B*) Dose–response of the mCherry fluorescence (*Left*) and the cpGFP fluorescence (*Middle*) from purified ratiometric gCarvi protein. The cpGFP and mCherry fluorescences were normalized to the value in the absence of cAMP. cpGFP, but not mCherry, fluorescence increased upon cAMP binding. Dose–response curves of the cpGFP/mCherry ratio for cAMP (closed circle) and cGMP (open triangle). Fitting curves for cAMP (solid line) and cGMP (dashed line) were calculated with the Hill equation. Each ratio intensity was normalized to the R_{min}. (n = 3 independent experiments). (*C*) Summary table of ratiometric gCarvi properties. The dissociation constants for cAMP and cGMP were 2.05 ± 0.06 μM and 28.9 ± 2.5 μM, respectively. The Hill constants for cAMP and cGMP were 1.36 ± 0.05 and 0.95 ± 0.07, respectively. The dynamic ranges for cAMP and cGMP were 1.50 ± 0.02 and 0.33 ± 0.01, respectively. The binding rate and unbinding rate constants for cAMP were 1.20 ± 0.32 × 10^6 M^{-1} s^{-1} and 3.11 ± 0.84 s^{-1} (n = 8 independent experiments). (*D*) Representative image of ratiometric gCarvi-expressing cultured hippocampal neuron (19 DIV). (Scale bar, 20 μm.) (*E*) Representative time profile of ratiometric gCarvi expressing neuron permeabilized with escin (30 μM) was exposed to cAMP at variable concentrations (1, 10, and 100 μM). (*F*) Dose–response curve of ratiometric gCarvi in cells (11 to 35 DIV, n = 18 cells). Data were obtained from 12 independent experiments. The fitting curve was calculated with the Hill equation (K_d = 3.20 ± 0.38 μM, n = 1.41 ± 0.13). Each ratio intensity was normalized to the R_{min}. Basal cAMP concentration in hippocampal neuron was estimated to be 1.38 ± 0.59 μM (open star). All data represent the means ± SD.

minutes after washout of the drugs, FM 4-64 was reloaded, and second imaging was conducted (Fig. 4*D*). Like cAMP signals, FM-dye ratio in individual presynaptic boutons varied in intensities (Fig. 4*E*), and there was a positive correlation between the magnitude of cAMP elevation and the ratio of FM-dye intensities (Fig. 4*F*, $r = 0.84$, $P < 0.001$). In agreement with our results, FSK induced a long-term increase in the size of the recycling SV pool in cultured cerebellar granule cells for 30 to 60 min after washout of the drug (39, 40). Thus, individual boutons possess presynaptic cAMP domains for compartmentalized signaling pathways, thereupon establishing synaptic strengthening without cross-talk.

Discussion

Utility of the Monomeric cAMP Indicator gCarvi. We have developed a green fluorescent cAMP indicator, gCarvi. This indicator is bright enough to monitor cAMP kinetics in single cells even at single presynaptic boutons. Compared with FRET-based cAMP indicators, this probe is easy handling for cAMP imaging under the conditions with little change in intracellular pH and can be readily converted to a ratiometric probe or a probe specifically targeted to a particular subcellular compartment. Since gCarvi is constructed from a bacterial CBD with <30% amino acid homology to mammalian CBDs (23),

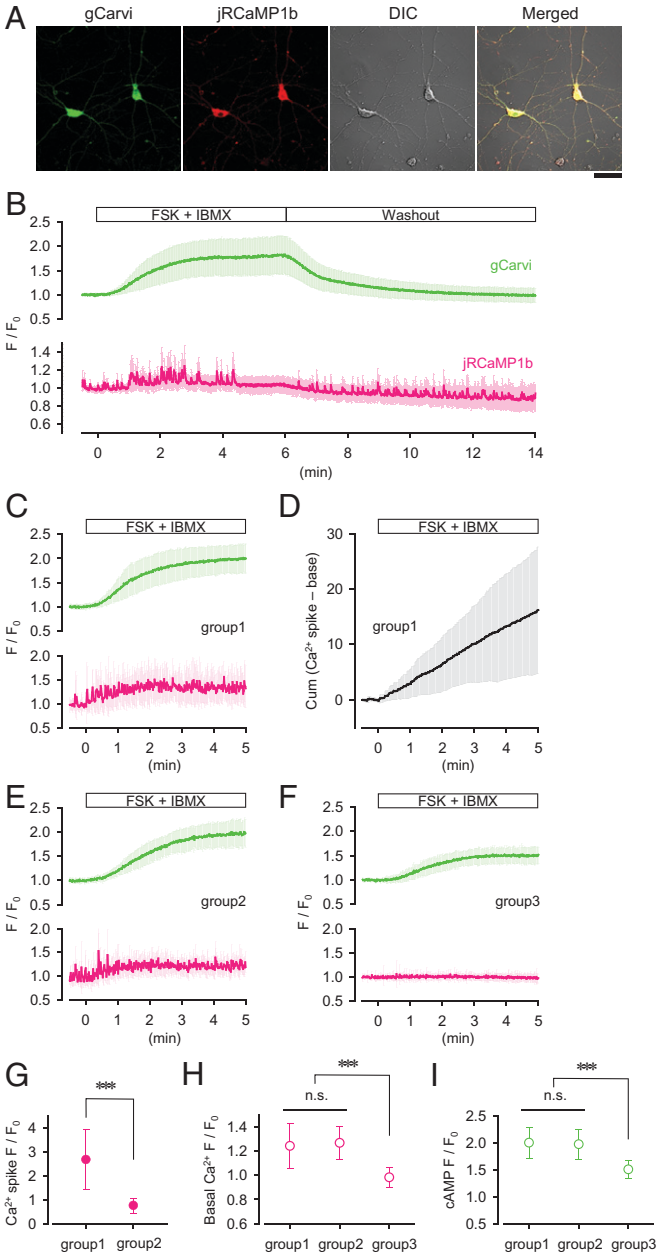

Fig. 3. Simultaneous detection of cAMP and Ca^{2+} dynamics in hippocampal neurons. (*A*) gCarvi (green)- and jRCaMP1b-expressing (red) hippocampal neuron in culture (17 DIV). (Scale bar, 50 μm.) (*B*) Mean time profile of gCarvi (in green) and jRCaMP1b (in red) during 10 μM FSK with 100 μM IBMX-stimulating phase and subsequent washout phase at hippocampal soma (17 to 19 DIV, $n = 11$ cells). Data were obtained from five independent experiments. Each fluorescence intensity was normalized to the mean baseline value before application. (*C*) Of the 57 neurons tested (17 to 32 DIV; data were obtained from 11 independent experiments), 25 (group 1) showed an increase in spontaneous bursts of somatic Ca^{2+} spikes during cAMP elevation. (*D*) Cumulative plot of the variation in Ca^{2+} spike generation from *C* indicates that cAMP elevation induced robust Ca^{2+} spike generation. (*E*) Another 17 neurons (group 2) showed a concomitant tonic increase in Ca^{2+} with cAMP. (*F*) The remaining 15 neurons (group 3) showed relatively small increases in cAMP in response to FSK/IBMX and no clear change in the level of Ca^{2+}. (*G*) Comparison of induced rates of Ca^{2+} spikes by FSK/IBMX between group 1 (2.67 ± 1.25) and group 2 (0.76 ± 0.31, ***$P < 0.001$, unpaired t test). (*H*) basal Ca^{2+} changes of group 1 (1.24 ± 0.19) and group 2 (1.27 ± 0.14) stimulated by FSK/IBMX are similar ($P = 0.863$. n.s., not significant) and larger than that of group 3 (0.98 ± 0.08, ***$P < 0.001$, ANOVA with post hoc Tukey's tests). (*I*) FSK/IBMX-induced cAMP elevations of group 1 (1.99 ± 0.29) and group 2 (1.96 ± 0.27) are similar ($P = 0.938$. n.s., not significant) and larger than that of group 3 (1.50 ± 0.17, ***$P < 0.001$, ANOVA with post hoc Tukey's tests). All data represent the means ± SD.

it is unlikely to perturb cAMP pathways in mammalian cells. gCarvi has a D.R. for cAMP of ~1.5 with a K_d of ~2 μM, covering 0.2 to 20 μM with one ligand binding stoichiometry. Since $[cAMP]_i$ reportedly increases up to 20 μM (16, 17, 28, 29, 35, 41–44) by Gs protein-coupled receptors stimulation without PDE inhibitor, gCarvi can reliably detect the physiological range of cAMP changes in many cells. Regarding a buffering effect of the probe, 1 μM gCarvi can theoretically capture 0.3 μM cAMP at basal (1.4 μM) $[cAMP]_i$ and 1 μM cAMP at 20 μM $[cAMP]_i$ levels. These buffering effects should be taken into account when studying rapid cAMP transients and diffusions.

The basal $[cAMP]_i$ of <100 nM was reported in 293A cells (44), whereas higher levels in the range of 0.8 to 3 μM have been reported in many other cell types (29, 34, 35, 44–46). Using ratiometric gCarvi, our estimate for the basal $[cAMP]_i$ level in hippocampal neurons was 1.4 μM. Although half maximal effective concentration (EC_{50}) values of various PKAs in vitro are reportedly in the submicromolar range (47, 48), using PKA and PKA substrate–based FRET probes, Koschinski and Zaccolo reported that the EC_{50} of intracellular PKA is 5 μM with a Hill coefficient of 2 (34). Indeed, PKA activity in hippocampal neurons is reported to be low at the basal $[cAMP]_i$ (49, 50). Furthermore, this estimation fits well with the K_d of PDE4, limiting the level of hippocampal basal $[cAMP]_i$ (51, 52).

In developing neurons, the balance between cAMP and cGMP is essential for neurite differentiation (53) and growth cone motility (54). In mature neurons, both cAMP and cGMP are involved in synaptic modulations (6). The operational concentration range of cGMP is 0.1 to 3 μM (20), which largely overlaps with that of cAMP. Therefore, to study cAMP dynamics with high selectivity, K_d for cGMP of a cAMP indicator should be preferably >30 μM. Except for gCarvi, among existing cAMP indicators, only Pink Flamindo meets this requirement (55). With respect to cAMP/cGMP specificity defined as the selectivity (K_d ratio) multiplied by the sensitivity (D.R. ratio), the specificity of gCarvi is 106, whereas that of Pink Flamindo is 13. The highest cAMP/cGMP specificity so far reported is 63 for the high-affinity indicator Epac2-camps300 (56) (*SI Appendix*, Table S4).

Physiological cAMP changes in response to neuronal activity can be faster than those induced by bath application of G protein-coupled receptors agonist or forskolin. In striatal spiny projection neurons, optical stimulation of dopaminergic input fibers induces robust spine enlargement via the cAMP–PKA signaling with a time window of 0.3 to 2 s (57). The Gs-coupled neuromodulation in learning processes is thought to have a time window of seconds (58–60). Estimating the time resolution of gCarvi using a microperfusion system, 10 μM cAMP gave an association time constant of 0.07 s and a dissociation time constant of 0.30 s. Therefore, gCarvi can be utilized for monitoring physiological cAMP changes in response to neuronal activities.

Utilization of Simultaneous Detection of cAMP and Ca^{2+}. The linkage between cAMP and Ca^{2+} signals has been discussed in a variety of neurons (36). By coexpressing gCarvi and the red Ca^{2+} indicator jRCaMP1b in cultured hippocampal neurons, we found that large cAMP increases induced by FSK/PDE inhibitor was accompanied by marked increases in Ca^{2+} dynamics. An increase in Ca^{2+} spikes associated with cAMP transients was first described in *Xenopus* embryonic spinal neurons (61). In cultured hippocampal neurons, pituitary adenylate cyclase–activating polypeptide increases Ca^{2+} spikes (62), which might be dependent

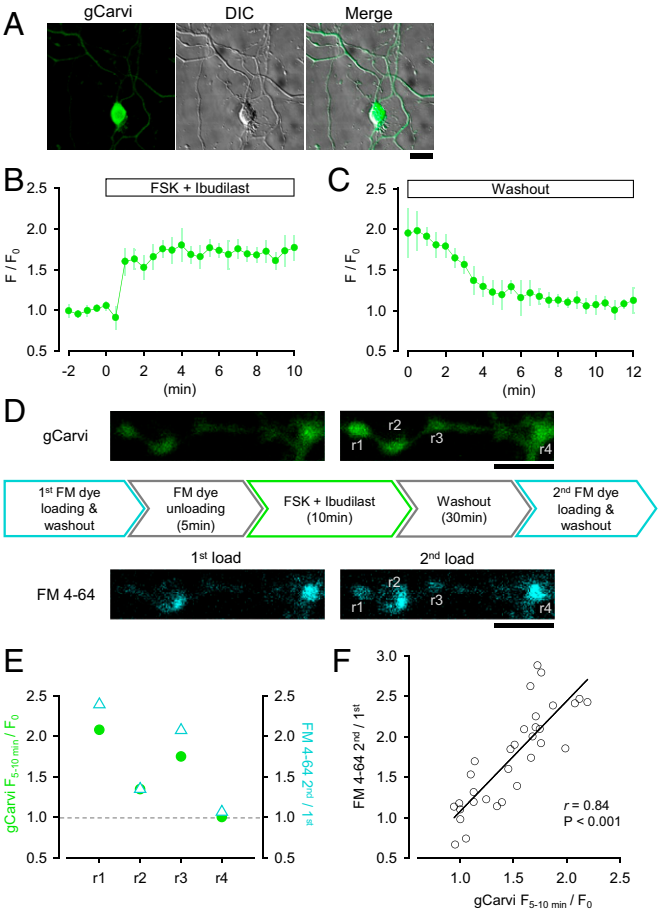

Fig. 4. Correlation analysis of recycling pool size and cAMP increase at individual boutons. (*A*) gCarvi-expressing (green) cerebellar granule cell (15 DIV). (Scale bar, 20 μm.) Mean time profile of gCarvi during 10 μM FSK with 50 μM ibudilast stimulating (*B*) and subsequent washout phase (*C*) at individual bouton in cerebellar granule cell culture. Data were obtained from four independent experiments (n = 27 boutons, 15 cells). gCarvi fluorescence was normalized to the mean value before application. (*D*) Experimental paradigm to evaluate recycling pool size before and after cAMP elevation (*Middle*). Representative images of gCarvi in presynaptic boutons before (*Top Left*) and during (*Top Right*) FSK/ibudilast application. (Scale bar, 10 μm.) Neurons were stimulated by depolarization with a high KCl (72 mM) solution for 5 min in the presence (loading) or absence (unloading) of FM 4-64. After loading, peripheral dye was washed out for 15 min. Loaded FM 4-64 images at the same boutons before (*Bottom Left*, first load) and after (*Bottom Right*, second load) cAMP elevation. (Scale bar, 10 μm.) (*E*) The fluorescence changes of gCarvi (closed circle in green) and FM 4-64 (open triangle in blue) at the boutons as in *D*. (*F*) Correlation plot of between gCarvi and FM 4-64 changes. Data were obtained from four independent experiments (n = 32 boutons, 15 cells). Pearson analysis indicated the linear correlation between two parameters (r = 0.84, P < 0.001). All data represent the means ± SD.

on activation of glutamate receptors via PKA phosphorylation (63). Our cAMP/Ca^{2+} dual imaging showed that $[cAMP]_i$ elevation in hippocampal neurons can also trigger increasing basal Ca^{2+}. cAMP elevation reportedly increases Ca^{2+} influx through L-type Ca^{2+} channels (64) or Ca^{2+} release through IP3 receptor activation (65), both of which might cause tonic Ca^{2+} increase in hippocampal neurons. Simultaneous cAMP/Ca^{2+} monitoring using gCarvi may reveal kinetic differences between $[Ca^{2+}]_i$ elevations mediated by distinct mechanisms.

Intraterminal cAMP Can Determine Presynaptic Plasticity. In cerebellar GC–PC synapses, FSK induces presynaptic-long term potentiation (pre-LTP), which occludes tetanic stimulation–induced pre-LTP (38). The cAMP–PKA pathway also presynaptically activates silent synapses (39, 40). In this study, FSK/PDE inhibitor increased recycling pool size in GC presynaptic boutons assayed using FM-dye uptake after the prolonged washout in agreement with previous reports (39, 40). Furthermore, we found that cAMP elevations, which varied widely among presynaptic boutons, positively correlated with subsequent increases in recycling pool size. These results suggest that presynaptic cAMP domains may play a key role in presynaptic plasticity that can be revealed by live imaging of cAMP with gCarvi.

Materials and Methods

Ethical Approval. All experiments were performed in accordance with the guidelines of Doshisha University.

Chemicals. Cyclic AMP, cyclic GMP, the other nucleotides, (3-mercaptopropyl) trimethoxysilane and Escin were purchased from Sigma. Nickel (II) sulfate hexahydrate IBMX, ibudilast, and forskolin were purchased from Fujifilm. Maleimido-C3-NTA was purchased from Dojindo. Potassium methanesulfonate was purchased from Tokyo Chemical Industry. Fluorescein reference standard was purchased from Invitrogen.

Plasmid Construction. Green fluorescent cAMP indicators were constructed as follows: cAMP-binding domains of *E. coli* (DH5α) CRP (amino acids 1 to 129 … 138, or 156, GenBank accession No. KP670514) and the cpGFP of GCaMP3 (amino acids 61 to 301, GenBank accession No. HM143847) were amplified by PCR. The series of cpGFP mutants was generated via PCR-based site-directed mutagenesis using the cpGFP of GCaMP3 as template. These PCR products were inserted into subcloning vector pBluescript II KS(+) (Agilent) followed by sequence analysis. cpGFPs were fused to the *Xho*I site attached to the C terminal of CBDs. CBD-cpGFP constructs were inserted to pCold I (TaKaRa) for protein expression in *E. coli*, gCarvi (CBD-cpGFP) construct was inserted into pAAV1-hSynapsin promoter, and pAAV2-SynTetOff (33) for protein expression in cerebellar granule cell and hippocampal neuron, respectively. pmCherry-C1 (Clontech) and pTagRFP-C (Evrogen) were used for the construction of mCherry-CBD-cpGFP and TagRFP-CBD-cpGFP, respectively.

Bacterial Protein Expression and Purification. *E. coli* BL21 (BioDynamics) transformed with histidine tag–containing pCold I-gCarvi was grown at 37 °C until OD_{600} ~0.4, and protein expression was induced by adding 0.5 mM isopropyl β-D-thiogalactoside and incubating for an additional 20 to 24 h at 15 °C. Protein-expressing *E. coli* were lysed with BugBuster solution (Merck), followed by binding with Talon cobalt resin (Clontech). According to the manufacturer's batch procedure, proteins were eluted with buffer containing 50 mM Na-phosphate, 300 mM NaCl, and 150 mM imidazole. Subsequently, proteins were concentrated and the buffer was replaced with phosphate-buffered saline (PBS) by passing through a high molecular weight cut filter (>10,000 kDa, VIVASPIN 6, Sartorius). The concentrated protein solutions were stored at 4 °C under dark conditions. For screening of gCarvi and ratiometric gCarvi, fluorescence (excitation filter = 485 nm [bandwidth = 20 nm]/emission filter = 535 nm [20 nm] for cpGFP fluorescence and excitation = 560 nm [20 nm]/emission = 610 nm [20 nm] for red fluorescent proteins) of purified candidates was measured with or without cAMP or cGMP using a fluorescent microplate reader (Infinite F200, Tecan).

Optical Properties Analysis. Purified gCarvi protein was suspended in 50 mM Hepes buffer pH 7.0, containing 5 mM ascorbic acid, 4 mM glutathione, and 0.1% bovine serum albumin. The absorption spectra of purified gCarvi protein were measured using an ultraviolet (UV) spectrophotometer (UV-1800, Shimadzu), and the fluorescence spectra were measured using a fluorescence spectrophotometer (FP-6500, JASCO). Fluorescein reference standard (Invitrogen) was used for calibration of green fluorescent intensity. To make a titration curve of gCarvi, purified gCarvi protein was suspended in the following buffers: 50 mM acetate buffer for pH 4.5 and 5.0; 50 mM 2-morpholinoethanesulfonic acid buffer for pH 5.5, 6.0, and 6.5; 50 mM Hepes buffer for pH 7.0, 7.5, and 8.0; and 50 mM Tris buffer for pH 8.5 and 9.0, each supplemented with 5 mM ascorbic acid, 4 mM glutathione, and 0.1% bovine serum albumin.

Binding Kinetics Analysis. Coverslips (No. 1s, 18 mmΦ, Matsunami) were washed with 1% acetic acid solution for 6 h. The coverslips were immersed in silanized solution containing 50% ethanol, 2% mercaptosilane, and 1% acetic acid overnight, then dried at 143 °C for 1 h. Then, the coverslips were immersed sequentially in reducing solution containing 50% ethanol, 2.5 mM ethylenediaminetetraacetic acid, 2 mM dithiothreitol, and 100 mM phosphate buffer, pH = 7.0 for 1 h, 2.5 mg/mL maleimido-C3-NTA solution for 2 h, and 50 mM $NiSO_4$ solution for 1 h. The Ni complexed coverslip was incubated with 100 μg purified gCarvi or ratiometric gCarvi in 10 mL PBS to bind, and stored at 4 °C until use. gCarvi or a ratiometric gCarvi binding coverslip was placed on the stage of a confocal microscope (LSM 710, Zeiss) and superfused with PBS or cAMP-containing PBS using a microperfusion system (μflow, ALA Scientific Instruments). Their fluorescence was measured using a line-scan mode (1.89 ms/line) with a 20×, 0.8 numerical aperture (N.A.) dry objective lens. Argon 488 nm and DPSS 561 nm were used for excitation of cpGFP and mCherry, respectively. Emissions were collected between 493 nm and 556 nm for cpGFP and 600 nm and 696 nm for mCherry.

Primary Cell Culture. Cerebella were dissected from Institute of Cancer Research (ICR) mouse at embryonic day 18 (E18). Cerebellar neurons were dissociated using Neuron Dissociation Solutions (Fujifilm) and plated on coverslips coated with poly-D-lysine (Sigma) at a density of 10^5 cells/cm^2 in neurobasal medium supplemented with 2% B27 (Gibco), 2 mM L-alanyl-L-glutamine (Fujifilm), and 22 mM KCl. Dissociated neurons were maintained at 37 °C in 5% CO_2 for 15 days in vitro (DIV). Hippocampi were dissected from ICR embryos at E16 to E18. Hippocampal neurons were dissociated by using Neuron Dissociation Solutions and plated on coverslips coated with poly-D-lysine at a density of 4×10^4 cells/cm^2 in neurobasal medium supplemented with B27 and 2 mM L-alanyl-L-glutamine. Dissociated neurons were maintained at 37 °C in 5% CO_2 for 11 DIV and later. The protocols for animal experiments have been approved by the Doshisha University Animal Research Committee #A18022, #A19010, #A20064 and #A21044.

AAV Preparation. pAAVs, pRC1, and pHelper (TaKaRa) were cotransfected into HEK293T cells (American Type Culture Collection) by calcium phosphate transfection (Promega). The medium was replaced 6 h after transfection with Dulbecco's modified Eagle's medium (Fujifilm) containing 10% fetal bovine serum (Gibco). The medium containing virus particles was collected 48 h after medium replacement and subsequently filtered through a PVDF membrane (Millex-HV, Millipore). AAV particles were concentrated by AAVanced concentration reagent (System Biosciences) according to the manual's protocol. The virus solution was stored in aliquots at −80 °C until use. rAAV-hSyn-gCarvi was added to cultures of cerebellar granule cell at 3 DIV. rAAV-SynTetOff-gCarvi and rAAV-hSyn-jRCaMP1b (#100851; Addgene) were added to hippocampal neuronal cultures at 3 to 6 DIV. rAAV-SynTetOff-ratiometric gCarvi was added to cultures of hippocampal neuron at 3 to 6 DIV.

Live Cell Imaging. Experiments were performed in Hank's balanced salt solution (HBSS, Fujifilm) unless otherwise noted. For cerebellar granule cell experiments, images were taken using a confocal microscopy (LSM710, Zeiss) with a 20×, 0.8 N.A. dry objective lens. Argon 488 nm was used for excitation both of cpGFP and FM 4-64 (Invitrogen). Emissions were collected between 493 nm and 556 nm for cpGFP or 661 nm and 759 nm for FM 4-64. Repeated FM 4-64 loading resulted in $F_{second}/F_{first} = 1.24 \pm 0.19$ (*SI Appendix*, Fig. S12). Therefore, 0.24 has been subtracted from the second intensities in the analysis of Fig. 4 *E* and *F* for correction. Time-lapse images were acquired every 30 s using Zen 2009 software (Zeiss). A total of 5 μM FM 4-64 was loaded and unloaded with high KCl solution containing (in millimoles) 71.6 NaCl, 71.6 KCl, 1.26 $CaCl_2$, 0.49 $MgCl_2$, 0.40 $MgSO_4$, 4.17 $NaHCO_3$, 0.44 KH_2PO_4, 0.34 Na_2HPO_4, and 5.6 glucose. A total of 10 μM forskolin and 50 μM ibudilast dissolved in HBSS were bath applied to cerebellar neurons using a perfusion system. For experiments using gCarvi/jRCaMP1b-expressing hippocampal neuron, cells were imaged at 17 to 32 DIV using a confocal microscopy (TCS SP5, Leica) with a 20×, 1.0 N.A. water immersion objective lens. Argon 488 nm and He-Ne 543 nm were used for excitation of cpGFP and mCherry, respectively. Emissions were collected between 496 nm and 535 nm for cpGFP, and 571 nm and 700 nm for mCherry. Time-lapse images were acquired every 0.74 s using LAS AF software (Leica) and analyzed with LAS X software. A total of 10 μM forskolin and 100 μM IBMX dissolved in HBSS were bath applied to hippocampal neurons using a perfusion system. Platinum-iridium wires (#778000; A-M SYSTEMS) were connected to an electronic stimulator (15 V, 200-μs duration, SEN-7203, Nihon Kohden) for field electrical stimulation. For in-cell calibration of ratiometric gCarvi, hippocampal neurons were imaged at 11 to 35 DIV using a confocal microscopy (LSM710, Zeiss) with a 20×, 0.8 N.A. dry objective lens. Permeabilization solution contained (in millimoles) 0.03 escin, 120 potassium methanesulfonate, 20 NaCl, 0.55 $MgSO_4$, 1 ethylene glycol bis(β-aminoethylether)-tetraacetic acid (EGTA), and 40 Hepes/KOH pH 7.4. cAMP perfusion solutions contained (in millimoles) 0.01 escin, 120 potassium methanesulfonate, 20 NaCl, 0.55 $MgSO_4$, 1 EGTA, and 40 Hepes/KOH pH 7.4 supplemented with 1 μM, 10 μM, or 100 μM cAMP. Time-lapse images were acquired every 5 s, and subsequently analyzed with Zen 2009 software (Zeiss). The optimal pH (7.4) of the permeabilization solution was determined using mCherry-cpGFP–expressing hippocampal neurons (*SI Appendix*, Fig. S13).

Data Analysis. The 3D structure of gCarvi was predicted using the Phyre2 web portal for protein modeling (66) and viewed with iCn3D (67). In the case of styryl dye experiments, fluorescence image data were analyzed with Fiji (68). Any other images were processed with Zen 2009 software or LAS X software. Line-scan data for binding kinetics analysis were processed with GraphPad Prism 6J. The data shown represent the means ± SD. Mean values were compared by *t* test or one-way ANOVA with post hoc Tukey's multiple comparisons. Correlation was analyzed by Pearson correlation. These statistical analyses were calculated with SPSS Statistics 26 and $P < 0.05$ was considered significantly different.

Data Availability. All study data are included in the article and/or *SI Appendix*. Mendeley Data, V1, doi: 10.17632/xk9g24gcxb.1 (69).

ACKNOWLEDGMENTS. We thank T. Tanaka, K. Mitsuyasu, C. Ueda, and Y. Kubo for their experimental assistance; T. Hori for invaluable experimental advice; and P. Stoney for English editing. We are also grateful to H. Hioki (Juntendo University) for kindly providing us pAAV2 SynTetOff vector (ref. 33). This work was supported by the Core Research for Evolutional Science and Technology of the Japan Science and Technology Agency (to T.T.), Grant-in-Aid for Scientific Research from Ministry of Education, Culture, Sports, Science and Technology Japan (26640031 and 23500403), and a Doshisha Harris Grant (to N.S.).

1. J. C. Chang, R. P. J. Oude-Elferink, Role of the bicarbonate-responsive soluble adenylyl cyclase in pH sensing and metabolic regulation. *Front. Physiol.* **5**, 42 (2014).
2. D. M. F. Cooper, V. G. Tabbasum, Adenylate cyclase-centred microdomains. *Biochem. J.* **462**, 199–213 (2014).
3. A. T. Bender, J. A. Beavo, Cyclic nucleotide phosphodiesterases: Molecular regulation to clinical use. *Pharmacol. Rev.* **58**, 488–520 (2006).
4. M. Zaccolo, A. Zerio, M. J. Lobo, Subcellular organization of the cAMP signaling pathway. *Pharmacol. Rev.* **73**, 278–309 (2021).
5. A. Pfeifer, A. Kilić, L. S. Hoffmann, Regulation of metabolism by cGMP. *Pharmacol. Ther.* **140**, 81–91 (2013).
6. E. K. Argyrousi, P. R. A. Heckman, J. Prickaerts, Role of cyclic nucleotides and their downstream signaling cascades in memory function: Being at the right time at the right spot. *Neurosci. Biobehav. Rev.* **113**, 12–38 (2020).
7. G. Grynkiewicz, M. Poenie, R. Y. Tsien, A new generation of Ca^{2+} indicators with greatly improved fluorescence properties. *J. Biol. Chem.* **260**, 3440–3450 (1985).
8. S. R. Adams, A. T. Harootunian, Y. J. Buechler, S. S. Taylor, R. Y. Tsien, Fluorescence ratio imaging of cyclic AMP in single cells. *Nature* **349**, 694–697 (1991).
9. M. J. Berridge, M. D. Bootman, H. L. Roderick, Calcium signalling: Dynamics, homeostasis and remodelling. *Nat. Rev. Mol. Cell Biol.* **4**, 517–529 (2003).
10. M. J. Berridge, Elementary and global aspects of calcium signalling. *J. Physiol.* **499**, 291–306 (1997).
11. J. Y. Jiang, J. L. Falcone, S. Curci, A. M. Hofer, Interrogating cyclic AMP signaling using optical approaches. *Cell Calcium* **64**, 47–56 (2017).
12. N. Kim, S. Shin, S. W. Bae, cAMP biosensors based on genetically encoded fluorescent/luminescent Proteins. *Biosensors (Basel)* **11**, 39 (2021).
13. N. C. Surdo *et al.*, FRET biosensor uncovers cAMP nano-domains at β-adrenergic targets that dictate precise tuning of cardiac contractility. *Nat. Commun.* **8**, 15031 (2017).
14. A. Bock *et al.*, Optical mapping of cAMP signaling at the nanometer scale. *Cell* **182**, 1519–1530.e17 (2020).
15. K. Gorshkov *et al.*, AKAP-mediated feedback control of cAMP gradients in developing hippocampal neurons. *Nat. Chem. Biol.* **13**, 425–431 (2017).
16. B. J. Bacskai *et al.*, Spatially resolved dynamics of cAMP and protein kinase A subunits in *Aplysia* sensory neurons. *Science* **260**, 222–226 (1993).
17. S. R. Neves *et al.*, Cell shape and negative links in regulatory motifs together control spatial information flow in signaling networks. *Cell* **133**, 666–680 (2008).

18. D. Lee, Global and local missions of cAMP signaling in neural plasticity, learning, and memory. *Front. Pharmacol.* **6**, 161 (2015).
19. B. Trivedi, R. H. Kramer, Real-time patch-cram detection of intracellular cGMP reveals long-term suppression of responses to NO and muscarinic agonists. *Neuron* **21**, 895–906 (1998).
20. M. Thunemann *et al.*, Transgenic mice for cGMP imaging. *Circ. Res.* **113**, 365–371 (2013).
21. O. Ros *et al.*, SponGee: A genetic tool for subcellular and cell-specific cGMP manipulation. *Cell Rep.* **27**, 4003–4012.e6 (2019).
22. E. Fic *et al.*, cAMP receptor protein from *Escherichia coli* as a model of signal transduction in proteins–A review. *J. Mol. Microbiol. Biotechnol.* **17**, 1–11 (2009).
23. J. B. Shabb, J. D. Corbin, Cyclic nucleotide-binding domains in proteins having diverse functions. *J. Biol. Chem.* **267**, 5723–5726 (1992).
24. N. Popovych, S. R. Tzeng, M. Tonelli, R. H. Ebright, C. G. Kalodimos, Structural basis for cAMP-mediated allosteric control of the catabolite activator protein. *Proc. Natl. Acad. Sci. U.S.A.* **106**, 6927–6932 (2009).
25. H. Sharma, S. Yu, J. Kong, J. Wang, T. A. Steitz, Structure of apo-CAP reveals that large conformational changes are necessary for DNA binding. *Proc. Natl. Acad. Sci. U.S.A.* **106**, 16604–16609 (2009).
26. A. I. Kostyuk, A. D. Demidovich, D. A. Kotova, V. V. Belousov, D. S. Bilan, Circularly permuted fluorescent protein-based indicators: History, principles, and classification. *Int. J. Mol. Sci.* **20**, 4200 (2019).
27. Y. Zhao *et al.*, An expanded palette of genetically encoded Ca^{2+} indicators. *Science* **333**, 1888–1891 (2011).
28. S. L. Mironov *et al.*, Imaging cytoplasmic cAMP in mouse brainstem neurons. *BMC Neurosci.* **10**, 29 (2009).
29. B. S. Muntean *et al.*, Interrogating the spatiotemporal landscape of neuromodulatory GPCR signaling by real-time imaging of cAMP in intact neurons and circuits. *Cell Rep.* **22**, 255–268 (2018).
30. H. Urakubo, S. Yagishita, H. Kasai, S. Ishii, Signaling models for dopamine-dependent temporal contiguity in striatal synaptic plasticity. *PLoS Comput. Biol.* **16**, e1008078 (2020).
31. D. Ohadi, P. Rangamani, Geometric control of frequency modulation of cAMP oscillations due to calcium in dendritic spines. *Biophys. J.* **117**, 1981–1994 (2019).
32. S. Mukherjee *et al.*, A novel biosensor to study cAMP dynamics in cilia and flagella. *eLife* **5**, e14052 (2016).
33. J. Sohn *et al.*, A single vector platform for high-level gene transduction of central neurons: Adeno-associated virus vector equipped with the tet-off system. *PLoS One* **12**, e0169611 (2017).
34. A. Koschinski, M. Zaccolo, Activation of PKA in cell requires higher concentration of cAMP than in vitro: Implications for compartmentalization of cAMP signalling. *Sci. Rep.* **7**, 14090 (2017).
35. R. V. Iancu *et al.*, Cytoplasmic cAMP concentrations in intact cardiac myocytes. *Am. J. Physiol. Cell Physiol.* **295**, C414–C422 (2008).
36. S. Averaimo, X. Nicol, Intermingled cAMP, cGMP and calcium spatiotemporal dynamics in developing neuronal circuits. *Front. Cell. Neurosci.* **8**, 376 (2014).
37. H. Dana *et al.*, Sensitive red protein calcium indicators for imaging neural activity. *eLife* **5**, e12727 (2016).
38. P. A. Salin, R. C. Malenka, R. A. Nicoll, Cyclic AMP mediates a presynaptic form of LTP at cerebellar parallel fiber synapses. *Neuron* **16**, 797–803 (1996).
39. P. Chavis, P. Mollard, J. Bockaert, O. Manzoni, Visualization of cyclic AMP-regulated presynaptic activity at cerebellar granule cells. *Neuron* **20**, 773–781 (1998).
40. M. A. Cousin, G. J. O. Evans, Activation of silent and weak synapses by cAMP-dependent protein kinase in cultured cerebellar granule neurons. *J. Physiol.* **589**, 1943–1955 (2011).
41. L. I. Jiang *et al.*, Use of a cAMP BRET sensor to characterize a novel regulation of cAMP by the sphingosine 1-phosphate/G13 pathway. *J. Biol. Chem.* **282**, 10576–10584 (2007).
42. P. S. Salonikidis, A. Zeug, F. Kobe, E. Ponimaskin, D. W. Richter, Quantitative measurement of cAMP concentration using an exchange protein directly activated by a cAMP-based FRET-sensor. *Biophys. J.* **95**, 5412–5423 (2008).
43. J. D. Violin *et al.*, β2-adrenergic receptor signaling and desensitization elucidated by quantitative modeling of real time cAMP dynamics. *J. Biol. Chem.* **283**, 2949–2961 (2008).
44. S. Börner *et al.*, FRET measurements of intracellular cAMP concentrations and cAMP analog permeability in intact cells. *Nat. Protoc.* **6**, 427–438 (2011).
45. P. Hockberger, T. Yamane, Compartmentalization of cyclic AMP elevation in neurons of *Aplysia californica*. *Cell. Mol. Neurobiol.* **7**, 19–33 (1987).
46. J. Y. Jiang, J. L. Falcone, S. Curci, A. M. Hofer, Direct visualization of cAMP signaling in primary cilia reveals up-regulation of ciliary GPCR activity following Hedgehog activation. *Proc. Natl. Acad. Sci. U.S.A.* **116**, 12066–12071 (2019).
47. J. A. Beavo, P. J. Bechtel, E. G. Krebs, Activation of protein kinase by physiological concentrations of cyclic AMP. *Proc. Natl. Acad. Sci. U.S.A.* **71**, 3580–3583 (1974).
48. K. Taskén, E. M. Aandahl, Localized effects of cAMP mediated by distinct routes of protein kinase A. *Physiol. Rev.* **84**, 137–167 (2004).
49. J. Z. Young, C. Isiegas, T. Abel, P. V. Nguyen, Metaplasticity of the late-phase of long-term potentiation: A critical role for protein kinase A in synaptic tagging. *Eur. J. Neurosci.* **23**, 1784–1794 (2006).
50. T. Abel *et al.*, Genetic demonstration of a role for PKA in the late phase of LTP and in hippocampus-based long-term memory. *Cell* **88**, 615–626 (1997).
51. M. Barad, R. Bourtchouladze, D. G. Winder, H. Golan, E. Kandel, Rolipram, a type IV-specific phosphodiesterase inhibitor, facilitates the establishment of long-lasting long-term potentiation and improves memory. *Proc. Natl. Acad. Sci. U.S.A.* **95**, 15020–15025 (1998).
52. R. Havekes *et al.*, Compartmentalized PDE4A5 signaling impairs hippocampal synaptic plasticity and long-term memory. *J. Neurosci.* **36**, 8936–8946 (2016).
53. M. Shelly *et al.*, Local and long-range reciprocal regulation of cAMP and cGMP in axon/dendrite formation. *Science* **327**, 547–552 (2010).
54. T. Kobayashi, F. Nagase, K. Hotta, K. Oka, Crosstalk between second messengers predicts the motility of the growth cone. *Sci. Rep.* **3**, 3118 (2013).
55. K. Harada *et al.*, Red fluorescent protein-based cAMP indicator applicable to optogenetics and in vivo imaging. *Sci. Rep.* **7**, 7351 (2017).
56. R. P. Norris *et al.*, Cyclic GMP from the surrounding somatic cells regulates cyclic AMP and meiosis in the mouse oocyte. *Development* **136**, 1869–1878 (2009).
57. S. Yagishita *et al.*, A critical time window for dopamine actions on the structural plasticity of dendritic spines. *Science* **345**, 1616–1620 (2014).
58. K. Lee *et al.*, Temporally restricted dopaminergic control of reward-conditioned movements. *Nat. Neurosci.* **23**, 209–216 (2020).
59. K. He *et al.*, Distinct eligibility traces for LTP and LTD in cortical synapses. *Neuron* **88**, 528–538 (2015).
60. Y. Yovell, T. W. Abrams, Temporal asymmetry in activation of *Aplysia* adenylyl cyclase by calcium and transmitter may explain temporal requirements of conditioning. *Proc. Natl. Acad. Sci. U.S.A.* **89**, 6526–6530 (1992).
61. Y. V. Gorbunova, N. C. Spitzer, Dynamic interactions of cyclic AMP transients and spontaneous $Ca^{(2+)}$ spikes. *Nature* **418**, 93–96 (2002).
62. Z. Liu *et al.*, Frequency modulation of synchronized Ca^{2+} spikes in cultured hippocampal networks through G-protein-coupled receptors. *J. Neurosci.* **23**, 4156–4163 (2003).
63. I. V. Sokolova, H. A. Lester, N. Davidson, Postsynaptic mechanisms are essential for forskolin-induced potentiation of synaptic transmission. *J. Neurophysiol.* **95**, 2570–2579 (2006).
64. E. T. Kavalali, K. S. Hwang, M. R. Plummer, cAMP-dependent enhancement of dihydropyridine-sensitive calcium channel availability in hippocampal neurons. *J. Neurosci.* **17**, 5334–5348 (1997).
65. S. C. Tovey, C. W. Taylor, Cyclic AMP directs inositol (1,4,5)-trisphosphate-evoked Ca^{2+} signalling to different intracellular Ca^{2+} stores. *J. Cell Sci.* **126**, 2305–2313 (2013).
66. L. A. Kelley, S. Mezulis, C. M. Yates, M. N. Wass, M. J. E. Sternberg, The Phyre2 web portal for protein modeling, prediction and analysis. *Nat. Protoc.* **10**, 845–858 (2015).
67. J. Wang *et al.*, iCn3D, a web-based 3D viewer for sharing 1D/2D/3D representations of biomolecular structures. *Bioinformatics* **36**, 131–135 (2020).
68. J. Schindelin *et al.*, Fiji: An open-source platform for biological-image analysis. *Nat. Methods* **9**, 676–682 (2012).
69. S. Kawata, Y. Mukai, Y. Nishimura, T. Takahashi, N. Saitoh. Green fluorescent cAMP indicator of high speed and specificity suitable for neuronal live-cell imaging. Mendeley Data. https://data.mendeley.com/datasets/xk9g24gcxb/1. Deposited 22 June 2022.